Draft version September 11, 2026
Typeset using LaTeX **default** style in AASTeX7.0.1

Nitrogen-Loud Quasars from the Dark Energy Spectroscopic Instrument. I. Sample Selection and Basic Properties

Shuo Zhai [1] Wei-jian Guo [1] Yong-Jie Chen [2] Zhi-Qiang Chen [3] Haining Li [1,4] Jian-Min Wang [5,1,4] and Gang Zhao [1,4]

[1] National Astronomical Observatories, Chinese Academy of Sciences (CAS), Beijing 100101, P. R. China, gzhao@nao.cas.cn, lhn@nao.cas.cn
[2] Technology and Engineering Center for Space Utilization, Chinese Academy of Sciences, Beijing 100094, P. R. China
[3] School of Physics and Technology, Nanjing Normal University, No. 1, Wenyuan Road, Nanjing 210023, People's Republic of China
[4] School of Astronomy and Space Science, University of Chinese Academy of Sciences, 19A Yuquan Road, Beijing 100049, P. R. China
[5] Key Laboratory for Particle Astrophysics, Institute of High Energy Physics, Chinese Academy of Sciences, 19B Yuquan Road, Beijing 100049, P. R. China

ABSTRACT

We present the largest sample to date of nitrogen-loud (N-loud) quasars with strong broad N IV] λ1486 and/or N III] λ1750 emission lines over the redshift range $1.6 < z < 4.3$, selected from the Dark Energy Spectroscopic Instrument (DESI) Data Release 1. The final sample contains 1,993 N-loud quasars, corresponding to about 1.2% of the parent quasar sample. The L_{1450} distribution of the N-loud quasars is broadly similar to that of the DESI parent sample, but their redshift distribution is distinct, with a stronger concentration around $z \sim 2.5$–3. Their composite spectrum displays a broadly similar UV continuum shape to that of the parent quasars, while showing significantly enhanced broad nitrogen emission features, including N V, N IV], and N III]. Other metal emission features also show a moderate enhancement. Relative to a control sample matched in redshift and UV continuum luminosity, the N-loud quasars show systematically narrower broad C IV and Mg II emission lines, lower single-epoch virial black hole masses, and higher Eddington ratios, suggesting that N-loud quasars may preferentially appear during a relatively rapid black hole accretion phase. The radio-loud fraction is 10.1%, with the highest fraction among objects exhibiting both N III] and N IV] emission. The catalog provides a statistical baseline for future studies of nitrogen enhancement and its physical origin.

Keywords: Active galactic nuclei (16) — Active galaxies (17) — Quasars (1319) — Catalogs (205)

1. INTRODUCTION

Nitrogen-loud (N-loud) quasars,[6] characterized by unusually strong broad nitrogen emission lines, form a rare but recognizable subclass of quasars. The best-known example is Q0353−383, whose spectrum exhibits prominent N IV] λ1486, N III] λ1750, and N V λ1240 emission lines (P. S. Osmer 1980). Such objects have long been used to investigate chemical enrichment in the broad line region (BLR), since strong nitrogen emission is generally thought to be associated with anomalous chemical abundances, and may in particular reflect enhanced nitrogen abundance or high metallicity (J. A. Baldwin et al. 2003; N. D. Batra & J. A. Baldwin 2014; K. Matsuoka et al. 2017). In recent years, with the rapid progress of James Webb Space Telescope observations of chemically peculiar sources at high redshift, strong nitrogen emission and its physical origin have again attracted broad attention (A. J. Bunker et al. 2023; X. Ji et al. 2024, 2026; Y. Isobe et al. 2025). Although these high-redshift sources are not necessarily identical to the classical N-loud quasars, a well-defined low- to intermediate-redshift N-loud quasar sample can provide an important reference for understanding the strong-nitrogen phenomenon and a statistical basis for future abundance analyses based on broad emission lines.

[6] Quasars with strong broad N III] and/or N IV] emission lines have historically been referred to as both N-rich and N-loud quasars. In this paper, we adopt the term N-loud quasars consistently, while retaining the original terminology when referring to previous studies.

Systematic searches based on the Sloan Digital Sky Survey (SDSS) gradually established N-loud quasars as a rare spectroscopic subclass. M. C. Bentz & P. S. Osmer (2004) first identified 16 candidate nitrogen-enriched quasars in the SDSS Early Data Release, initiating a systematic search for such objects. M. C. Bentz et al. (2004) subsequently reported 20 N-rich quasars in the SDSS First Data Release, corresponding to about 0.4% of the sample. L. Jiang et al. (2008) further identified 293 quasars with strong N IV] or N III] emission over the redshift range $1.7 < z < 4.0$, providing the first statistically meaningful sample of N-loud quasars. N. D. Batra & J. A. Baldwin (2014) then carried out BLR metallicity analyses for 43 objects with the strongest N IV] and N III] emission, finding that these sources tend to have high BLR metallicities and relatively low black hole masses. In addition to the SDSS-based optical studies, K. Matsuoka et al. (2017) obtained near-infrared spectroscopy for 12 N-loud quasars and used rest-frame optical emission lines to further investigate their chemical properties and accretion states. These studies have revealed several important features of N-loud quasars, but the existing samples remain limited in size, data homogeneity, and selection strategy. In particular, the incidence of N-loud quasars relative to the parent quasar population, their redshift and luminosity distributions, their broad line and black hole properties, and their radio properties still require systematic characterization with a larger and more uniformly selected sample. Such a statistical baseline is also needed for further assessing the physical origin of the strong nitrogen emission.

In addition to these statistical limitations, the abundance pattern underlying the strong nitrogen emission remains ambiguous. A common interpretation links strong N V, N IV], and N III] emission to high metallicity, because nitrogen is expected to behave mainly as a secondary element at high metallicity, with N/O and N/C increasing with the overall metal abundance. In this framework, J. A. Baldwin et al. (2003) argued that the very high N/O inferred for the extreme N-rich quasar Q0353−383 implies very high overall metallicity, and N. D. Batra & J. A. Baldwin (2014) reached a similar conclusion from broad line analyses. However, strong nitrogen lines do not uniquely require an overall metallicity increase. Using near-infrared rest-frame optical spectra, K. Matsuoka et al. (2017) found that some N-loud quasars have [O III] λ5007 strengths comparable to those of normal quasars, rather than the strongly suppressed [O III] emission expected for extremely metal-rich narrow line region gas. This suggests that strong broad nitrogen lines do not necessarily indicate extremely high overall metallicity, but may instead reflect nitrogen enhancement relative to oxygen and other elements. Therefore, strong N III] or N IV] emission alone cannot distinguish between high overall metallicity and selective nitrogen enhancement; this requires multi-line abundance diagnostics and dedicated photoionization modeling based on a uniformly selected sample.

The large, homogeneous spectroscopic database and broad wavelength coverage of Dark Energy Spectroscopic Instrument (DESI) allow us to search for broad N IV] λ1486 and N III] λ1750 emission simultaneously over a wide redshift range, thereby enabling a new statistical study of N-loud quasars (DESI Collaboration et al. 2016a). This paper is the first in a series on DESI N-loud quasars, and focuses on constructing the sample and characterizing its basic statistical properties. We construct an N-loud quasar catalog based on DESI Data Release 1 (DR1) and measure their redshifts, UV continuum luminosities, equivalent width (EW) and FWHM of the major broad emission lines, single-epoch virial black hole masses, and Eddington ratios. We further characterize the radio properties of the sample through cross-matching with radio surveys. In the next paper of this series, we will use multiple UV emission line ratios and photoionization models to examine the abundance pattern of the sample, testing whether the strong nitrogen emission reflects an overall increase in metallicity or selective nitrogen enhancement relative to other elements.

The paper is organized as follows. In Section 2, we describe the DESI DR1 data, the construction of the parent sample, the N-loud quasar selection procedure, and the spectral fitting used to measure the relevant emission line properties. In Section 3, we present the basic properties of the selected N-loud quasars and compare their spectral, black hole, and radio properties with control samples. Our main conclusions are summarized in Section 4. Throughout this paper, we adopt a flat ΛCDM cosmology with $H_0 = 67.4$ km s^{-1} Mpc^{-1}, $\Omega_{\rm m} = 0.315$, and $\Omega_\Lambda = 0.685$ (Planck Collaboration et al. 2020).

2. DATA AND SAMPLE SELECTION

2.1. *DESI*

DESI is a Stage-IV wide-area ground-based multi-object spectroscopic survey mounted on the NOIRLab 4 m Mayall Telescope at Kitt Peak National Observatory (M. Levi et al. 2013; DESI Collaboration et al. 2016a,b, 2022; E. F. Schlafly et al. 2023). DESI is equipped with 5000 fibers and provides continuous wavelength coverage over 3600–9800 Å through three-arm spectrographs, with typical spectral resolutions of $\lambda/\Delta\lambda \sim 2100$, 3200, and 4100 for the three channels, respectively (T. N. Miller et al. 2024; J. H. Silber et al. 2023; DESI Collaboration et al. 2016b). We use spectra from DESI DR1, which includes observations obtained between 2021 May and 2022 June. The catalog spectra are coadded from multiple tiles or exposures, and the object classifications and redshift measurements are provided by the Redrock spectral template-fitting pipeline (A. Brodzeller et al. 2023).

We adopt the Redrock-based quasar classifications in DR1 as the starting point for constructing the parent sample, from which we further identify quasar candidates with unusually strong nitrogen emission lines. All spectra are corrected for Galactic extinction using the extinction curve of E. L. Fitzpatrick (1999) with $R_V = 3.1$, and are then shifted to the rest frame for the subsequent sample selection and emission line measurements.

2.2. *Sample Selection*

Our parent sample was constructed from the DESI DR1 catalog by selecting sources classified as quasars (`SPECTYPE=QSO`) and requiring `ZWARN=0`, thereby retaining only objects with reliable redshift measurements (DESI Collaboration et al. 2025). We further restricted the sample to the redshift range $1.6 \leq z \leq 4.3$, ensuring that both N IV] and N III] fall within the DESI wavelength coverage and can be analyzed simultaneously. To ensure sufficient continuum quality around the N III] region and to remain consistent with the selection criterion of M. C. Bentz et al. (2004), we required the continuum S/N > 5 in the rest-frame 1675–1725 Å window. The continuum S/N is defined as the ratio between the mean flux density and the mean flux uncertainty within this window. This window is adjacent to N III] and is relatively free of strong emission features. These criteria define the parent sample used for the subsequent selection, which contains 168,500 quasars.

We then identified N-loud quasar candidates from this parent sample in three steps, following the procedure illustrated in Figure 1. First, before performing the full spectral fitting, we used the local line S/N around N III] as a pre-selection metric. The local continuum was estimated from two sidebands on either side of N III], 1730–1740 Å and 1760–1770 Å, which are relatively free of strong emission features. We then computed the continuum-subtracted integrated flux within 1745–1755 Å and divided it by the propagated flux uncertainty in the same window to define the local line S/N. We required this local line S/N > 5 to remove spectra with no significant local excess around N III]. After this pre-selection, the sample was reduced to 11,661 quasars, corresponding to about 7% of the parent sample. This local S/N criterion is used only as an efficient pre-selection step to remove spectra without significant local excess near N III]. We did not compute an analogous local S/N around N IV], because this region lies close to C IV and is more easily contaminated by the broad C IV profile. Second, we performed spectral fitting for the pre-selected sources and measured the EW of N III] and N IV]; the fitting procedure and line measurements are described in Section 2.3. We retained objects with rest-frame EW > 3 Å in either N III] or N IV]. This threshold was adopted for two reasons: (1) for spectra passing the above local line S/N pre-selection, a nitrogen line with EW = 3 Å corresponds to a detection significance greater than 5σ, thus removing most spurious features caused by noise fluctuations; and (2) this threshold is consistent with the criteria used in previous N-loud quasar searches, facilitating direct comparison between the DESI sample and earlier SDSS-based samples (M. C. Bentz et al. 2004; L. Jiang et al. 2008). Finally, all fitted spectra were visually inspected to confirm the presence of nitrogen emission and to remove spurious cases caused by absorption features, noise spikes, or poor local continuum subtraction. The final sample contains 1,993 N-loud quasars, corresponding to about 1.2% of the parent sample; the resulting catalog is presented in Table 1.

2.3. *Spectral Fitting and Line Measurements*

To obtain uniform line measurements for the N-loud quasar selection and for the subsequent statistical characterization, we performed spectral fitting for the 11,661 sources that passed the local line S/N pre-selection described in Section 2.2. We fitted the spectra with DASpec (P. Du et al. 2018), a spectral decomposition code that employs the Levenberg–Marquardt algorithm to minimize χ^2 and fits all spectral components simultaneously, over the rest-frame wavelength range from 1450 Å to the maximum rest-frame wavelength allowed by the DESI observed-frame coverage. Based on whether the Mg II and Fe II regions remain within the DESI observed-frame wavelength coverage, we divided the fitted sources into three redshift intervals: for sources at $z < 2.37$, the fitting window includes both the Mg II and Fe II emission regions; for sources with $2.37 < z < 2.62$, the fitting includes the Fe II complex but excludes Mg II; and for sources at $2.62 < z < 4.3$, neither Mg II nor Fe II is included.

The pseudo-continuum and emission lines were fitted simultaneously. The continuum was modeled as a power law. Within the 1450–2000 Å region, the major emission lines N IV], C IV, N III], He II, and C III] were fitted with Gaussian profiles. Specifically, N III], N IV], He II, and C III] were fitted with single Gaussian profiles; for C IV, both single- and double-Gaussian models were considered, and the model with the lower reduced χ^2 was adopted. The C III] region

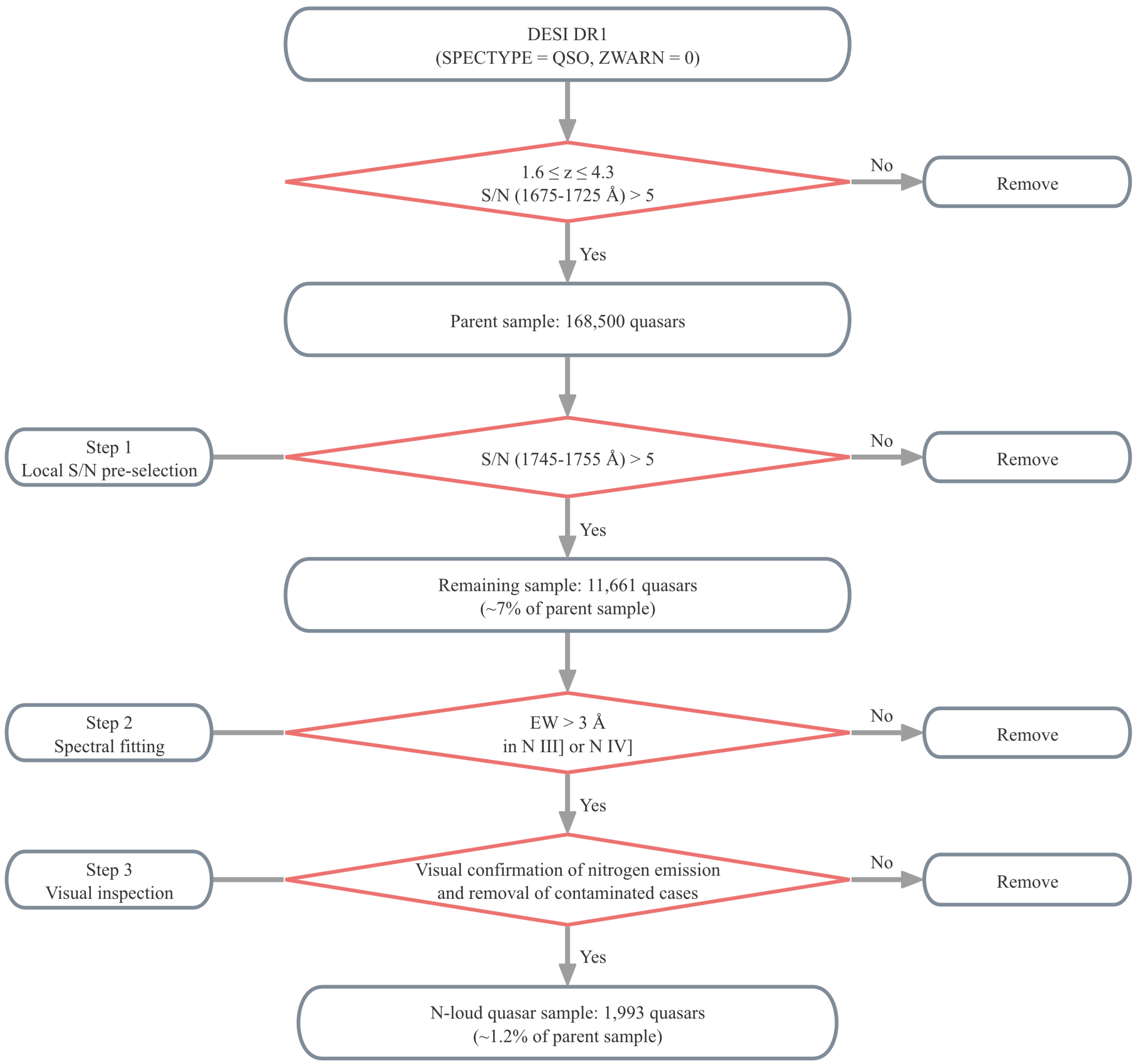

Figure 1. Selection flowchart for the DESI DR1 N-loud quasar sample. Starting from DESI DR1 quasars with `SPECTYPE=QSO` and `ZWARN=0`, we first require $1.6 \leq z \leq 4.3$ and S/N(1675–1725 Å) > 5, yielding a parent sample of 168,500 quasars. We then apply a local S/N pre-selection requiring S/N(1745–1755 Å) > 5, leaving 11,661 objects. Candidates are further selected through spectral fitting with EW > 3 Å in N III] or N IV], followed by visual inspection to confirm genuine nitrogen emission and remove contaminated cases. The final sample contains 1,993 N-loud quasars, corresponding to $\sim$1.2% of the parent sample.

may be affected by nearby weak emission features, such as Al IIIλ1857 and Si III]λ1892, but we did not attempt a detailed decomposition of these weak components. Because the N-loud selection is based only on N III] and N IV], this simplified treatment of the C III] complex does not affect the sample definition. For sources whose fitting window covers the Fe II region, the Fe II emission was modeled using a broadened and scaled version of the M. Vestergaard & B. J. Wilkes (2001) template; for sources whose fitting window covers Mg II, the Mg II line was fitted with a single Gaussian profile.

The FWHM and EW are measured from the best fits. The EW of N III] and N IV] were used for the EW-based sample selection described in Section 2.2. We then visually inspected all fitted spectra that passed the EW threshold to confirm the presence of nitrogen emission and to remove cases in which the relevant nitrogen features were severely affected by absorption features, noise spikes, or poor local continuum subtraction. An example of the spectral decomposition is shown in Figure 2.

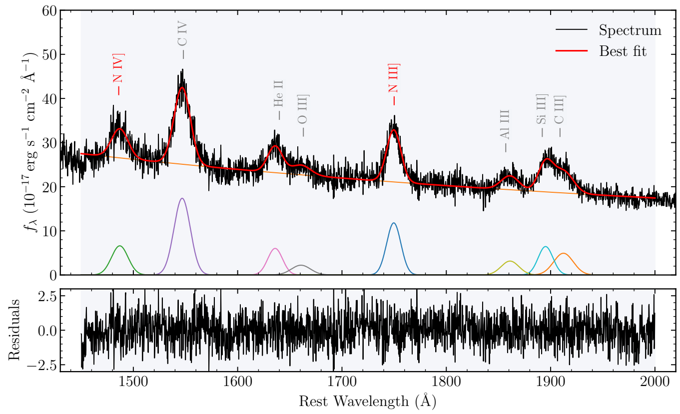

Figure 2. Spectral decomposition of an example N-loud quasar. The top panel shows the fitting result, and the bottom panel shows the residuals. The fitting window is indicated by the shaded region. The observed rest-frame spectrum is shown in black, and the total best-fit model is shown in red. The orange line shows the fitted continuum, and the individual emission line components are marked with different colored curves. The broad nitrogen features N IV] and N III], which define the N-loud selection, are highlighted in red.

3. RESULTS

Applying the selection procedure described in Section 2, we identify 1,993 N-loud quasars from the DESI DR1 quasar catalog over the redshift range $1.6 < z < 4.3$, corresponding to about 1.2% of the parent sample. The resulting catalog is presented in Table 1, including the source identifiers, coordinates, redshifts, continuum properties, major broad line measurements, and additional quantities derived from the spectral fitting.

In this section, we first summarize the sample composition and its distribution in redshift and luminosity (Section 3.1). We then examine the spectral properties of the N-loud quasars, including their nitrogen line properties, composite spectrum, and broad line properties relative to normal quasars (Section 3.2). Finally, we compare their single-epoch virial black hole masses and Eddington ratios with those of normal quasars (Section 3.3) and summarize their radio properties (Section 3.4).

3.1. *Basic Statistics*

The final sample consists of 1,993 N-loud quasars with different combinations of prominent nitrogen emission. Among them, 277 satisfy both the N III] and N IV] selection criteria, 1671 are selected only through strong N III], and 45 only through strong N IV]. Figure 3 shows four examples of the selected quasars. The first two spectra exhibit strong N III] and N IV] emission simultaneously, whereas the latter two are dominated mainly by strong N III] emission. Although the continuum shapes and the strengths of other emission features vary from object to object, prominent nitrogen emission is the defining feature of all selected sources.

Figure 4 first compares the location of the N-loud quasars and the DESI DR1 parent quasar sample in the z–L_{1450} plane[7]. The two samples occupy broadly similar regions in this parameter space, and their one-dimensional L_{1450} distributions are nearly identical, indicating that the selected N-loud quasars are not confined to a particular luminosity range. However, their one-dimensional redshift distributions differ, with the N-loud quasars more concentrated around $z \sim 2.5$–3.

Figure 5 then quantifies the observed fraction of N-loud quasars across the same z–L_{1450} parameter space. Consistent with the redshift-distribution difference shown in Figure 4, the observed N-loud fraction is not uniform with redshift: it increases from $z \sim 1.6$ to $z \sim 3$, reaches a peak of about 2%, and then declines toward higher redshift. By contrast, the dependence of the N-loud fraction on L_{1450} is weaker and should be interpreted with caution, especially in bins with

[7] We estimated the monochromatic luminosity $\lambda L_\lambda(1450\,\text{Å})$ from the median rest-frame continuum flux over 1440–1460 Å, using $\lambda L_\lambda(1450\,\text{Å}) = 4\pi D_L^2 \lambda f_\lambda(1450\,\text{Å})$. For simplicity, we denote $\lambda L_\lambda(1450\,\text{Å})$ as L_{1450} throughout this paper.

small parent-sample numbers. Because the detectability of weak nitrogen emission can depend on spectral quality, we further test in Section A whether the observed redshift dependence of the N-loud fraction is driven by the adopted continuum S/N cut. As shown in Figure 10, the same qualitative trend is recovered when the parent sample is redefined using stricter continuum S/N thresholds. This indicates that the observed redshift dependence is not primarily caused by the continuum S/N selection alone. Therefore, if this trend is not dominated by other selection effects, it may suggest a higher incidence of N-loud quasars around the epoch of peak quasar and galaxy activity.

The redshift-distribution difference between the DESI N-loud quasars and the DESI parent sample contrasts with the result of L. Jiang et al. (2008), whose N-rich quasar sample more closely follows the redshift distribution of the SDSS parent sample over a similar redshift range. This difference may partly reflect the different parent-sample definitions. L. Jiang et al. (2008) searched SDSS DR5 quasars with $1.7 < z < 4.0$ and $i < 20.1$, so their sample is closer to a brightness-limited census. In contrast, our DESI parent sample is defined by $1.6 < z < 4.3$ and further requires continuum S/N > 5 in the rest-frame 1675–1725 Å window, and is therefore more directly affected by spectral-quality requirements. Thus, the redshift distributions of the two N-loud samples should not be compared directly without accounting for the different parent-sample selection functions.

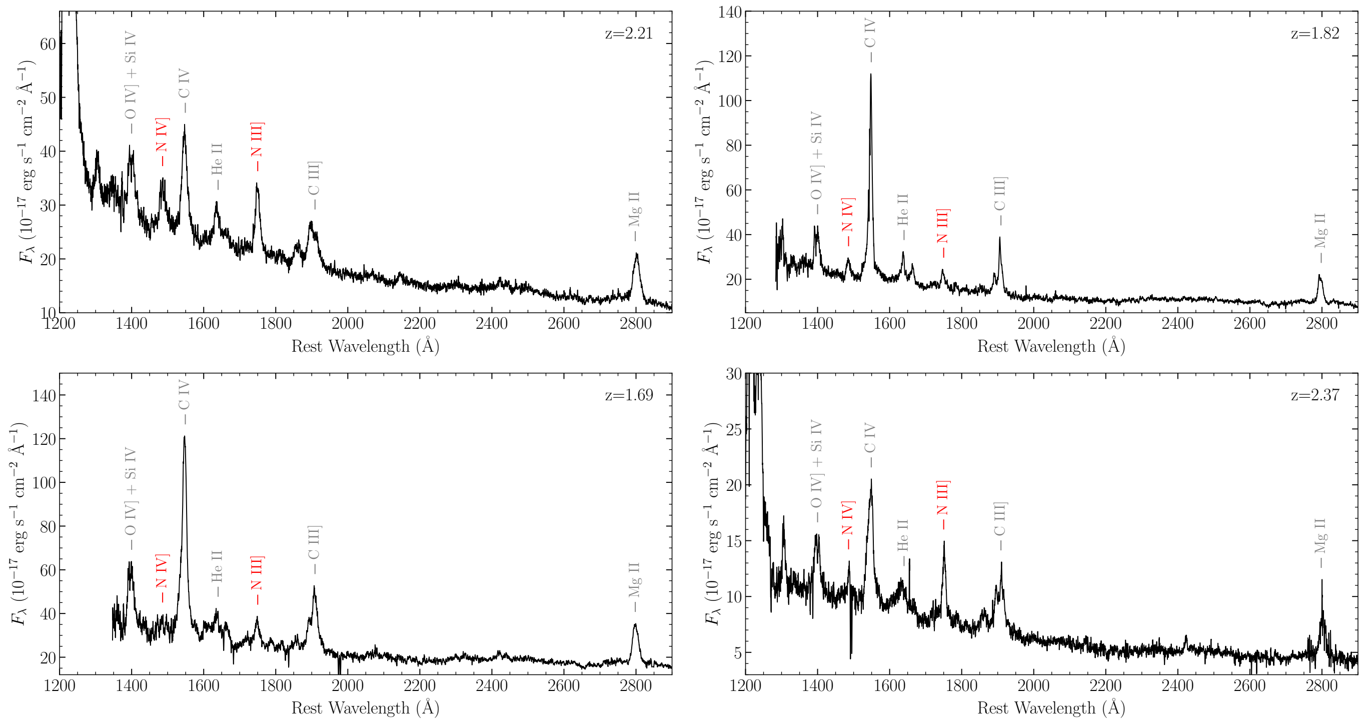

Figure 3. Example spectra of four N-loud quasars. The gray and black lines denote the original spectra and the spectra smoothed with a 5-pixel boxcar, respectively. The black dotted lines mark the positions of the N IV] and N III] lines. The two upper panels show quasars with strong N IV] and N III] lines, and the two lower panels show quasars with strong N III] lines.

3.2. *Spectral Properties*

To examine whether N-loud quasars differ from normal quasars in their overall UV continuum shape and major broad emission line features, we constructed composite spectra for the N-loud quasars and the DESI DR1 parent sample. All spectra were transformed to the rest frame and rescaled to a common continuum level at 1450 Å before combination. We adopted an unweighted average to reduce the influence of S/N differences among individual spectra. The resulting composites are shown in Figure 6. The two composites have broadly similar UV continuum shapes over most of the wavelength range, but several broad emission features are stronger in the N-loud composite. The most distinctive differences are the enhanced broad nitrogen features, including N V, N IV], and N III]. This indicates that the primary spectral signature of N-loud quasars is the systematic enhancement of nitrogen emission, possibly accompanied by a more general strengthening of metal emission lines.

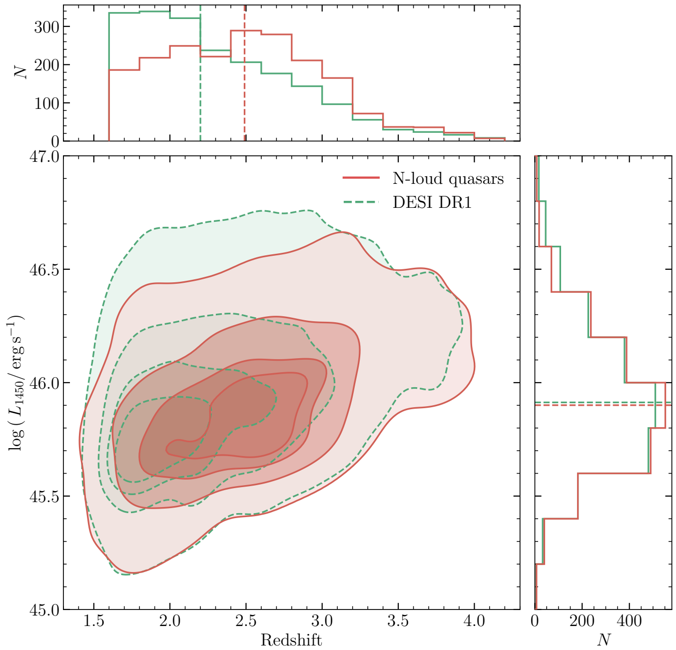

Figure 4. Redshift versus rest-frame 1450 Å luminosity distribution for the N-loud quasars and the DESI DR1 parent quasar sample. The 20%, 40%, 68%, and 95% percentile density contours are shown, with shaded regions indicating the corresponding density levels. Red solid contours represent the N-loud quasars, while green dashed contours represent the DESI DR1 parent quasar sample. The top and right panels show the corresponding one-dimensional distributions of redshift and $\log L_{1450}$, respectively, with dashed lines indicating the median values.

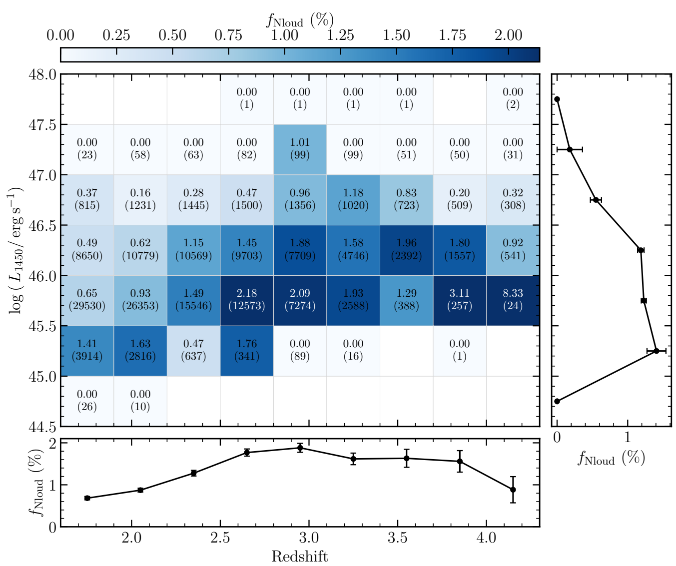

Figure 5. Observed fraction of N-loud quasars as functions of redshift and rest-frame 1450 Å luminosity. The numbers in parentheses are the total numbers of quasars in each bin, and only bins with N-loud quasar detections are shown. The bottom and right panels show the corresponding one-dimensional fractions as functions of redshift and $\log L_{1450}$, respectively, with error bars indicating the statistical uncertainties.

Figure 7 shows the distribution of the N III] EW and FWHM in the N-loud sample, providing a statistical characterization of the nitrogen line strength and width. We use N III] rather than N IV] as the main statistical line because N III] is detected in 98% of the final sample and lies in a relatively clean spectral region with less contamination from other strong emission lines. In contrast, N IV] lies close to C IV and is more easily affected by the broad C IV profile and local fitting uncertainties. Therefore, N III] serves as the primary statistical tracer of nitrogen emission in this sample. The N III] EW distribution peaks at about 4.0 Å, with a median of about 4.6 Å. The FWHM distribution peaks at about 3000 km s^{-1}, with a median of about 3600 km s^{-1}. Most objects are concentrated near these peak values, with the distributions extending toward larger EW and FWHM. Compared with L. Jiang et al. (2008), the EW distribution is broadly similar, while in their sample both the peak and median of the N III] FWHM distribution are near 4000 km s^{-1}, somewhat higher than in our sample.

Beyond the nitrogen lines, we further compared the major broad emission-line properties of N-loud quasars with those of normal quasars. Given that differences in redshift and luminosity distributions can affect direct comparisons of broad-line properties, we used an SDSS DR14 control sample matched to the DESI N-loud sample in redshift and UV continuum luminosity; the construction of this control sample is described in Appendix B. Figure 8 shows that the N-loud quasars are systematically shifted toward smaller EW and narrower FWHM in both C IV and Mg II, with the difference being more pronounced in FWHM. The median EW offsets are of order 10 Å, while the two samples cover broadly similar EW ranges. In contrast, the median FWHM offsets exceed 1000 km s^{-1}, and the N-loud quasars occupy a substantially narrower FWHM range, particularly for Mg II. A comparison between the N-loud quasars and a control sample matched to the DESI parent-quasar redshift–luminosity distribution also shows the same qualitative trend (Figure 13; Appendix C). This is also consistent with previous findings that the C IV and Mg II emission lines of N-loud quasars are narrower than those of typical quasars (M. C. Bentz et al. 2004; L. Jiang et al. 2008; K. Matsuoka et al. 2017). These independent comparisons consistently indicate that the non-nitrogen broad-line properties of N-loud quasars also differ systematically from those of normal quasars.

-

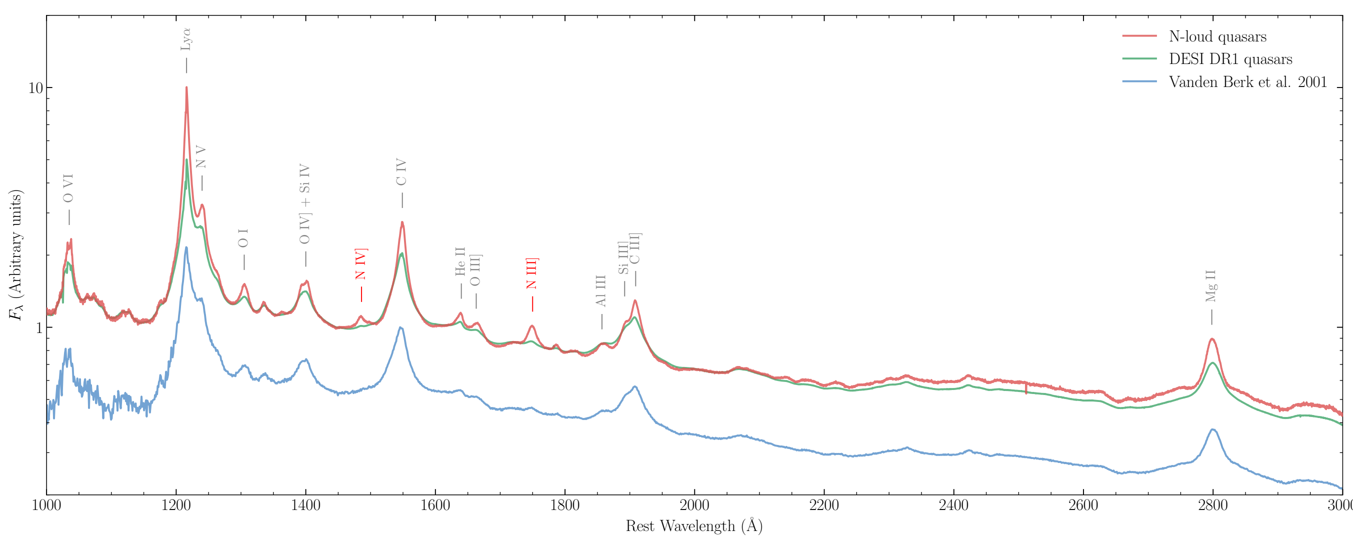

Figure 6. Composite spectra for the N-loud quasars (black) and DESI DR1 parent quasars (red). The dashed vertical lines mark the positions of the N IV] and N III] lines. For comparison, the blue curve denotes the composite spectrum of D. E. Vanden Berk et al. (2001).

3.3. *Black Hole Masses and Eddington Ratios*

Motivated by the systematically narrower C IV and Mg II broad lines of the N-loud quasars, we further estimated their single-epoch virial black hole masses and Eddington ratios. The black hole masses ($M_{\rm BH}$) were estimated using the broad Mg II and C IV emission lines. The Mg II estimator was adopted as the fiducial estimate whenever reliable Mg II measurements were available; otherwise, the C IV estimator was used. For the Mg II estimator, we adopted the calibration from M. Vestergaard & P. S. Osmer (2009),

$$\log\left(\frac{M_{\rm BH}}{M_\odot}\right) = 0.86 + 0.50\log\left(\frac{\lambda L_{3000}}{10^{44}\ {\rm erg\ s^{-1}}}\right) + 2\log\left(\frac{{\rm FWHM_{Mg\,II}}}{{\rm km\ s^{-1}}}\right). \quad (1)$$

For the C IV estimator, we adopted the calibration from M. Vestergaard & B. M. Peterson (2006),

$$\log\left(\frac{M_{\rm BH}}{M_\odot}\right) = 0.66 + 0.53\log\left(\frac{\lambda L_{1350}}{10^{44}\ {\rm erg\ s^{-1}}}\right) + 2\log\left(\frac{{\rm FWHM_{C\,IV}}}{{\rm km\ s^{-1}}}\right). \quad (2)$$

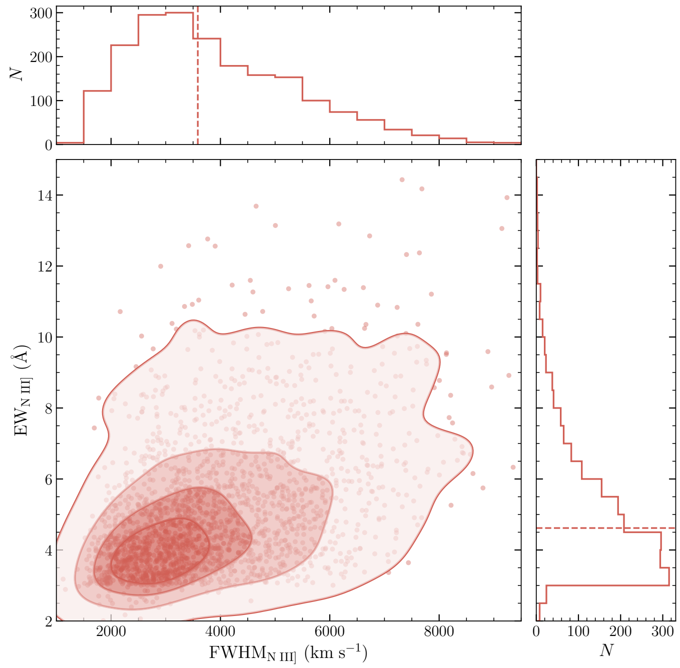

Figure 7. Rest-frame EW versus FWHM distribution of N III] for the N-loud quasars. Red points show individual objects. The 20%, 40%, 68%, and 95% contours and the corresponding density maps are shown. The top and right panels show the corresponding one-dimensional distributions of FWHM and EW, respectively, with dashed lines indicating the median values.

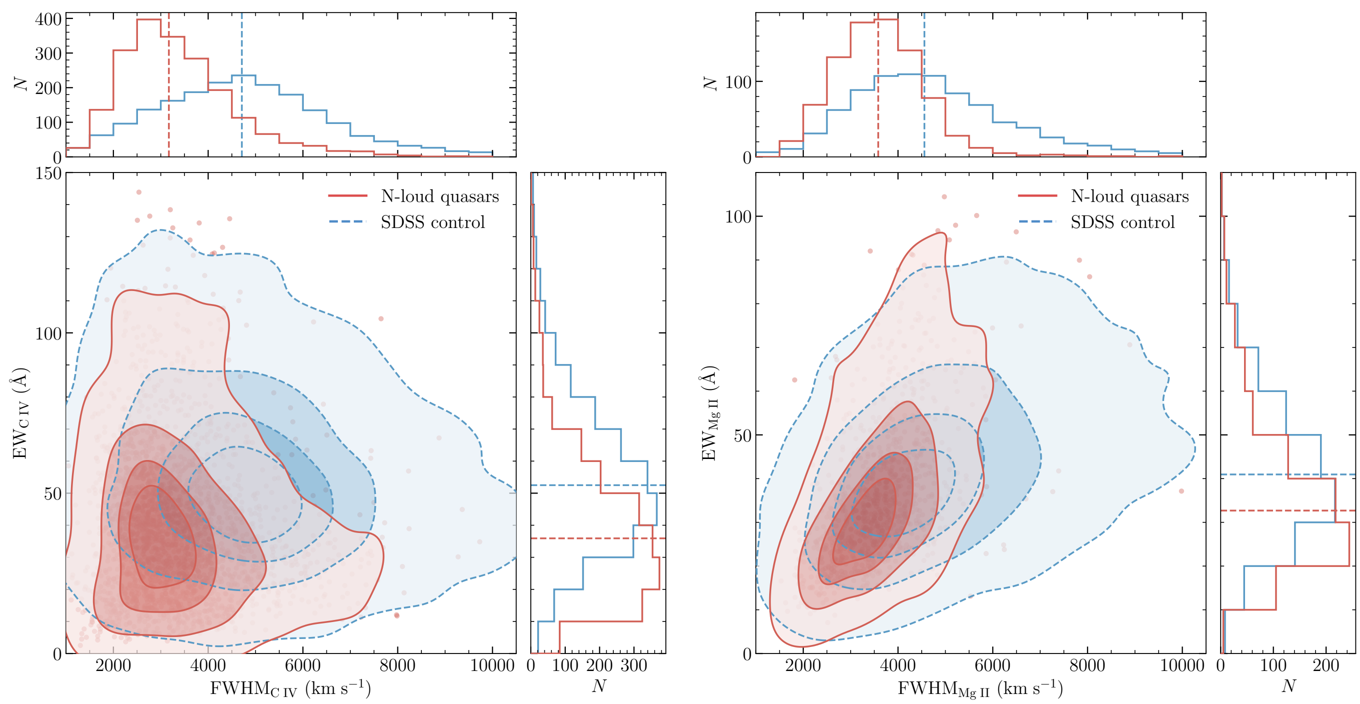

Figure 8. Rest-frame EW versus FWHM distributions of C IV (left panel) and Mg II (right panel) for the N-loud quasars (red solid contours) and SDSS DR14 control sample (blue dashed contours). Red points show individual objects. The 20%, 40%, 68%, and 95% contours and the corresponding density maps are shown. For each main panel, the top and right panels show the corresponding one-dimensional distributions of FWHM and EW, respectively, with dashed lines indicating the median values.

Here, λL_{3000} and λL_{1350} are the monochromatic continuum luminosities at 3000 and 1350 Å, respectively, and $\mathrm{FWHM}_{\mathrm{Mg\,II}}$ and $\mathrm{FWHM}_{\mathrm{C\,IV}}$ are the full widths at half maximum of the broad Mg II and C IV emission lines. The continuum luminosities and line widths were taken from our spectral measurements described in Section 3.1.

We further calculated the Eddington ratio as $\lambda_{\mathrm{Edd}} = L_{\mathrm{bol}}/L_{\mathrm{Edd}}$, where $L_{\mathrm{Edd}} = 1.26 \times 10^{38}(M_{\mathrm{BH}}/M_{\odot})\,\mathrm{erg\ s^{-1}}$. The bolometric luminosity was estimated from the monochromatic continuum luminosity at 1350 Å, $L_{\mathrm{bol}} = 3.81\,L_{1350}$, consistent with S. Rakshit et al. (2020).

We note that these single-epoch virial black hole masses are subject to substantial systematic uncertainties. In particular, C IV may be affected by non-virial components such as outflows, which can introduce additional scatter and bias relative to Mg II-based black hole mass estimates (L. Coatman et al. 2016, 2017). Therefore, the black hole masses and Eddington ratios derived here are used primarily for statistical characterization of the sample rather than for precise measurements of individual objects.

Figure 9 compares the M_{BH}–λ_{Edd} distributions of N-loud quasars and the SDSS control sample constructed in Appendix B. Although the two samples overlap substantially, their median values show that the N-loud quasars are systematically shifted toward lower black hole masses and higher Eddington ratios. The median $\log M_{\mathrm{BH}}/M_{\odot}$ of the N-loud quasars is about 8.75, approximately 0.25 dex lower than that of the SDSS control sample, while their median $\log \lambda_{\mathrm{Edd}}$ is about -0.3, approximately 0.3 dex higher. A comparison between the N-loud quasars and a control sample matched to the DESI parent-quasar redshift–luminosity distribution also shows the same qualitative trend (Figure 14; Appendix C). The black hole mass offset is also consistent with the systematically narrower C IV and Mg II broad lines shown in Figure 8, since single-epoch virial masses depend quadratically on line width. Overall, the N-loud quasars show a statistical trend toward lower black hole masses and higher Eddington ratios, consistent with previous studies (N. D. Batra & J. A. Baldwin 2014; K. Matsuoka et al. 2017).

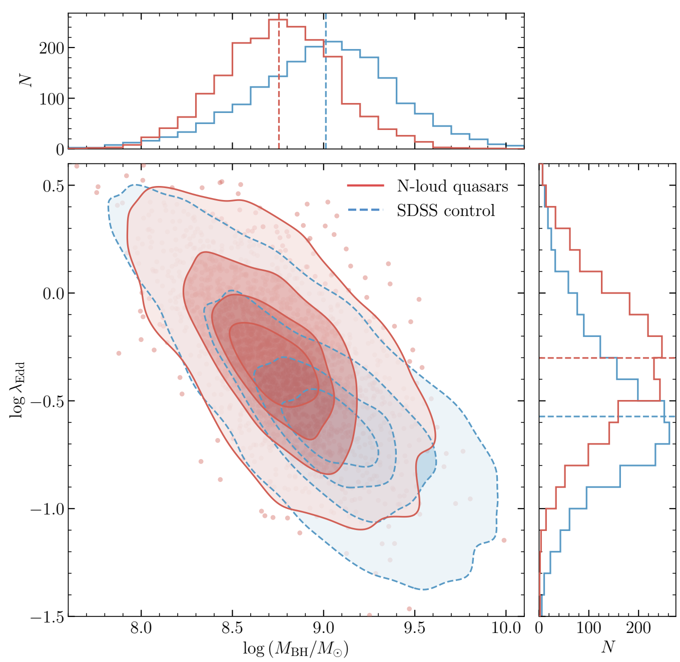

Figure 9. Black hole mass versus Eddington ratio distribution for the N-loud quasars and the SDSS control sample. The 20%, 40%, 68%, and 95% percentile density contours are shown, with shaded regions indicating the corresponding density levels. Red solid contours and points represent the N-loud quasars, while blue dashed contours represent the SDSS DR14 control sample. The top and right panels show the corresponding one-dimensional distributions of $\log M_{\mathrm{BH}}$ and $\log \lambda_{\mathrm{Edd}}$, respectively, with dashed lines indicating the median values.

3.4. *Radio Properties*

We investigated the radio properties of the N-loud sample by cross-matching our catalog with the Very Large Array Sky Survey (VLASS; M. Lacy et al. 2020) using a matching radius of 1.″5. A total of 203 N-loud quasars have VLASS counterparts under this criterion. The radio-loudness parameter is defined as $R = f_{6\,\mathrm{cm}}/f_{2500}$ (L. Jiang et al. 2007), where $f_{6\,\mathrm{cm}}$ is the rest-frame 6 cm flux density derived from the VLASS radio flux assuming a power-law radio slope of -0.7, and f_{2500} is the flux density at rest-frame 2500 Å. Quasars with $R > 10$ are classified as radio-loud. The VLASS peak fluxes and radio-loudness parameters for the matched sources are listed in Table 1.

Among the radio-detected sources, 202 satisfy this criterion, corresponding to a radio-loud fraction of $\sim 10.1\%$ for the full N-loud sample. The radio-loud fraction varies among the nitrogen line subtypes: it is $\sim 15.2\%$ for objects showing both N III] and N IV], $\sim 9.5\%$ for those with only N III], and $\sim 4.4\%$ for those with only N IV]. These subtype-dependent fractions should be interpreted with caution, especially for the N IV]-only class, which contains only a small number of objects. The radio-loud fraction derived here is substantially lower than that reported by L. Jiang et al. (2008). However, this contrast should not be interpreted as a direct discrepancy, because the two measurements are based on different parent samples and radio-selection procedures. The SDSS DR5 quasar catalog used by L. Jiang et al. (2008) was already coupled to the Faint Images of the Radio Sky at Twenty-cm survey (FIRST; R. H. Becker et al. 1995) at the candidate-selection stage, whereas the VLASS information in this work is added only after the N-loud sample is defined through catalog cross-matching. Overall, these results show that a non-negligible fraction of DESI N-loud quasars are radio-loud, with the highest radio-loud fraction found among objects showing both N III] and N IV] emission.

4. SUMMARY

We present a sample of 1,993 DESI DR1 quasars with strong broad N III] and/or N IV] emission lines at $1.6 < z < 4.3$, corresponding to about 1.2% of the parent quasar sample. The following points summarize our main findings:

1. The N-loud quasars have a L_{1450} distribution broadly similar to that of the DESI parent sample, but their redshift distribution differs from that of the parent sample. They are more concentrated around $z \sim 2.5$–3, and the observed N-loud fraction reaches a peak of about 2% near this redshift range.

2. The composite spectrum of the N-loud quasars has a broadly similar UV continuum shape to that of the parent quasars, while showing enhanced broad nitrogen emission lines, including N V, N IV], and N III]. Other metal emission features also show a moderate enhancement.

3. Relative to a control sample matched in redshift and UV continuum luminosity, the N-loud quasars systematically show narrower broad C IV and Mg II emission lines, lower single-epoch virial black hole masses, and higher Eddington ratios. These tendencies are also seen in comparison with the parent quasar sample. Relative to the matched control sample, the median $\log M_{\mathrm{BH}}$ of the N-loud quasars is lower by about 0.25 dex, while the median $\log \lambda_{\mathrm{Edd}}$ is higher by about 0.3 dex.

4. The radio-loud fraction of the N-loud quasars is 10.1%, with the highest fraction found in objects showing both N III] and N IV] emission.

Overall, these results indicate that N-loud quasars do not simply represent a small number of extreme objects in the distribution of nitrogen line strength, but instead show a set of correlated systematic properties, including a non-uniform redshift distribution, narrower broad emission lines, lower single-epoch virial black hole masses, higher Eddington ratios, and a non-negligible radio-loud subgroup. These properties suggest that N-loud quasars may preferentially appear during a relatively rapid black hole accretion phase. The consistent enhancement of multiple broad nitrogen emission lines also suggests that nitrogen enhancement is part of the overall UV spectral properties of these objects, rather than an isolated anomaly in a single line. The DESI N-loud quasar catalog presented here provides a large statistical baseline for future work. In the next paper of this series, we will use multiple UV emission lines and photoionization models to analyze their abundance patterns, testing whether the strong nitrogen emission reflects an overall increase in metallicity or selective nitrogen enhancement relative to other elements, and thereby further constraining the chemical-enrichment mechanism of N-loud quasars and its connection with black hole accretion state.

ACKNOWLEDGMENTS

S.Z. is grateful to C. Hu and P. Du for valuable discussions. This study is supported by the National Natural Science Foundation of China (NSFC) under grant No. 12588202, the Strategic Priority Research Program of the Chinese Academy of Sciences under grant No. XDB1160103, the National Key R&D Program of China under grant

Table 1. DESI DR1 N-loud quasar catalog

R.A.	Decl.	z	$\log L_{1450}$	α	EW (Å)				FWHM (km s^{-1})				Fe II/Mg II	Peak Flux	R
			(erg s^{-1})		N IV]	N III]	C IV	Mg II	N IV]	N III]	C IV	Mg II		(mJy beam^{-1})	
(1)	(2)	(3)	(4)	(5)	(6)	(7)	(8)	(9)	(10)	(11)	(12)	(13)	(14)	(15)	(16)
0.12	17.45	2.60	46.28 ± 0.01	-1.54 ± 0.01	...	3.3 ± 0.3	42.8 ± 1.5	...	...	2955 ± 307	3644 ± 284	...	...	...	...
0.14	3.66	3.22	46.32 ± 0.01	-1.22 ± 0.02	3.8 ± 0.5	3.7 ± 0.4	63.4 ± 1.3	...	5926 ± 763	4593 ± 486	3681 ± 347	...	...	...	...
0.70	-10.06	2.52	46.09 ± 0.01	-1.15 ± 0.03	2.2 ± 0.5	6.3 ± 0.4	26.6 ± 1.2	...	3711 ± 813	3169 ± 213	2646 ± 455	...	...	...	...
0.98	-0.04	2.49	45.89 ± 0.01	-1.30 ± 0.03	5.0 ± 0.5	4.4 ± 0.3	17.4 ± 0.5	...	4550 ± 462	1910 ± 148	3881 ± 113	...	...	...	...
1.43	5.86	2.03	45.80 ± 0.02	-1.66 ± 0.04	3.7 ± 0.5	5.4 ± 0.4	25.1 ± 1.5	17.4 ± 0.7	2052 ± 284	1913 ± 173	2181 ± 561	2733 ± 110	2.9 ± 0.3	...	...
1.45	19.89	3.17	45.92 ± 0.01	-1.85 ± 0.03	2.5 ± 0.3	3.5 ± 0.4	2.5 ± 0.3	...	1214 ± 170	1385 ± 187	1303 ± 192	...	...	99.3 ± 0.1	12795
1.62	16.26	1.97	45.66 ± 0.01	-1.83 ± 0.04	4.8 ± 0.8	11.3 ± 0.8	19.3 ± 1.6	19.5 ± 0.9	3254 ± 580	4594 ± 331	1556 ± 282	3085 ± 142	2.3 ± 0.3	...	...
1.64	1.66	2.81	45.99 ± 0.02	-0.49 ± 0.03	...	5.5 ± 0.6	15.4 ± 0.9	...	...	4153 ± 324	4153 ± 227	...	...	3.2 ± 0.2	103
1.70	-9.68	1.83	45.65 ± 0.02	-0.68 ± 0.05	0.7 ± 0.4	4.0 ± 0.5	67.6 ± 2.6	53.4 ± 1.6	1245 ± 917	2652 ± 350	3490 ± 281	4300 ± 65	3.5 ± 0.1	...	...
1.79	15.73	1.99	45.90 ± 0.02	-1.21 ± 0.02	2.5 ± 0.4	4.2 ± 0.3	67.8 ± 1.5	38.0 ± 1.0	2117 ± 339	2048 ± 169	2797 ± 213	3267 ± 48	4.1 ± 0.1	...	...
2.00	15.14	1.97	46.03 ± 0.01	-1.37 ± 0.02	3.9 ± 0.7	2.8 ± 0.4	62.8 ± 1.8	27.4 ± 0.8	5794 ± 1137	2667 ± 386	2297 ± 202	2832 ± 52	4.2 ± 0.2	...	...
2.30	0.97	2.70	46.02 ± 0.01	-1.55 ± 0.03	6.5 ± 0.8	2.0 ± 0.3	34.3 ± 0.6	...	8405 ± 1098	1858 ± 285	4875 ± 92	...	...	...	...
2.92	0.90	2.36	45.86 ± 0.01	-1.50 ± 0.02	3.2 ± 0.6	2.5 ± 0.3	45.0 ± 0.8	35.2 ± 1.5	6211 ± 1136	1786 ± 240	2110 ± 182	3712 ± 97	2.2 ± 0.2	...	...
3.01	2.31	3.53	46.41 ± 0.01	-1.29 ± 0.01	1.4 ± 0.2	4.7 ± 0.2	24.6 ± 0.2	...	2671 ± 393	3279 ± 186	2569 ± 24	...	...	...	...
3.25	-12.71	2.75	46.79 ± 0.02	-1.06 ± 0.01	...	4.9 ± 0.2	33.0 ± 0.5	...	...	6988 ± 337	2888 ± 120	...	...	...	...
3.25	-2.41	3.30	46.02 ± 0.01	-1.32 ± 0.03	1.3 ± 0.4	5.1 ± 0.6	37.6 ± 1.1	...	2202 ± 665	3741 ± 506	2115 ± 245	...	...	...	...
3.37	1.11	3.07	46.62 ± 0.01	-1.57 ± 0.01	...	3.6 ± 0.1	11.6 ± 0.4	...	...	6289 ± 915	4306 ± 91	...	...	...	...
3.75	20.97	3.10	46.09 ± 0.01	-1.53 ± 0.02	1.1 ± 0.4	5.4 ± 0.6	56.4 ± 1.5	...	1929 ± 707	5258 ± 693	2820 ± 344	...	...	...	...
4.03	0.59	3.07	45.74 ± 0.02	-1.19 ± 0.04	...	3.9 ± 0.5	78.7 ± 2.1	...	...	2782 ± 395	2562 ± 180	...	...	...	...
4.26	22.91	2.84	46.06 ± 0.01	-1.51 ± 0.02	2.5 ± 0.6	3.3 ± 0.3	28.8 ± 0.6	...	4693 ± 1272	2807 ± 301	1879 ± 35	...	...	...	...
4.40	-11.88	2.61	45.91 ± 0.01	-0.66 ± 0.03	2.5 ± 0.7	3.1 ± 0.4	55.9 ± 2.9	...	4524 ± 1311	2038 ± 296	3207 ± 362	...	...	...	...
4.53	4.26	2.00	45.72 ± 0.02	-1.85 ± 0.04	...	3.8 ± 0.6	25.9 ± 1.2	31.2 ± 1.2	...	2683 ± 463	6455 ± 282	3497 ± 130	4.5 ± 0.2	...	...
4.60	19.62	1.95	46.01 ± 0.01	-1.32 ± 0.02	0.3 ± 0.2	6.2 ± 0.6	17.9 ± 0.8	19.3 ± 0.5	523 ± 330	7780 ± 773	4500 ± 298	2592 ± 52	3.7 ± 0.3	...	...
4.86	10.53	2.11	46.17 ± 0.01	-1.00 ± 0.02	...	6.8 ± 0.4	51.7 ± 1.2	32.1 ± 0.7	...	5055 ± 449	4070 ± 233	3920 ± 55	2.8 ± 0.1	...	...
5.03	22.68	2.50	46.05 ± 0.01	-1.34 ± 0.03	...	4.2 ± 0.4	9.2 ± 0.7	...	...	2626 ± 307	3871 ± 295	...	...	2.3 ± 0.1	99
5.15	17.85	3.10	46.14 ± 0.01	-1.50 ± 0.02	...	5.0 ± 0.5	28.9 ± 1.6	...	...	4277 ± 436	3126 ± 298	...	...	...	...
5.62	23.16	1.75	45.67 ± 0.02	-1.54 ± 0.04	...	4.6 ± 0.5	62.1 ± 3.7	51.6 ± 2.3	...	1698 ± 224	2934 ± 380	2991 ± 69	2.9 ± 0.2	...	...
5.69	6.39	2.14	45.84 ± 0.01	-1.30 ± 0.02	...	3.2 ± 0.4	28.3 ± 1.7	30.2 ± 1.0	...	3055 ± 376	3422 ± 338	2921 ± 58	4.7 ± 0.2	...	...
6.09	0.77	2.01	45.99 ± 0.01	-0.81 ± 0.02	...	6.5 ± 0.5	11.4 ± 0.7	41.2 ± 1.0	...	7225 ± 902	7225 ± 413	3477 ± 41	4.9 ± 0.1	...	...
6.13	5.35	1.63	45.72 ± 0.02	-1.26 ± 0.02	...	3.0 ± 0.5	27.7 ± 0.6	19.2 ± 0.8	...	5402 ± 884	5002 ± 109	3483 ± 115	3.5 ± 0.3	...	...
6.55	-10.25	3.54	46.26 ± 0.01	-1.67 ± 0.03	1.3 ± 0.6	4.3 ± 0.4	48.0 ± 1.6	...	5190 ± 2440	2109 ± 207	2824 ± 233	...	...	...	...
6.91	-7.30	2.12	45.87 ± 0.02	-0.97 ± 0.02	0.6 ± 0.2	5.3 ± 0.3	44.0 ± 1.9	27.1 ± 0.6	771 ± 222	2661 ± 170	2735 ± 236	2693 ± 42	2.6 ± 0.2	...	...
6.94	11.49	2.86	46.02 ± 0.02	-1.50 ± 0.05	...	5.0 ± 0.5	23.3 ± 2.0	...	...	2399 ± 237	2009 ± 712	...	...	...	...

Notes. Column (1): R.A. Column (2): Decl. Column (3): redshift. Column (4): $\log L_{1450}$. Column (5): α. Columns (6)–(9): EW of N IV], N III], C IV, and Mg II. Columns (10)–(13): FWHM of N IV], N III], C IV, and Mg II. Column (14): Fe II/Mg II flux ratio, measured from the fitted Fe II UV pseudo-continuum and Mg II emission line. Column (15): peak flux at 3 GHz (mJy beam^{-1}). Column (16): radio loudness R. Table 1 is published in its entirety in the electronic edition. A portion is shown here for guidance regarding its form and content.

Nos. 2024YFA1611903, 2023YFE0107800, and 2024YFA1611601, and the CAS Project for Young Scientists in Basic Research under grant No. YSBR-092.

APPENDIX

A. ROBUSTNESS OF THE REDSHIFT EVOLUTION OF THE N-LOUD FRACTION TO CONTINUUM S/N CUTS

To test whether the observed redshift evolution of the N-loud fraction is affected by the continuum spectral quality of the parent quasar sample, we remeasured the N-loud fraction using different continuum S/N cuts, including S/N > 5, S/N > 10, and S/N > 15. In each redshift bin, we counted the numbers of parent quasars and N-loud quasars satisfying the corresponding continuum S/N criterion, and then calculated the N-loud fraction, with uncertainties estimated using the binomial approximation. Figure 10 shows the redshift dependence of the N-loud fraction obtained under different continuum S/N selections. The three curves show broadly consistent evolutionary behavior: the N-loud fraction increases from $z \sim 1.6$ to $z \sim 3$, reaches a peak around $z \sim 3$, and then declines toward higher redshift. Stricter continuum S/N cuts lead to larger uncertainties, especially at the high-redshift end, where the number of quasars with high continuum S/N becomes limited. Nevertheless, the overall redshift-dependent trend remains clearly visible under all three selections. The test indicates that the redshift evolution of the N-loud fraction is not primarily caused by the continuum S/N selection effect, but instead reflects a robust redshift dependence.

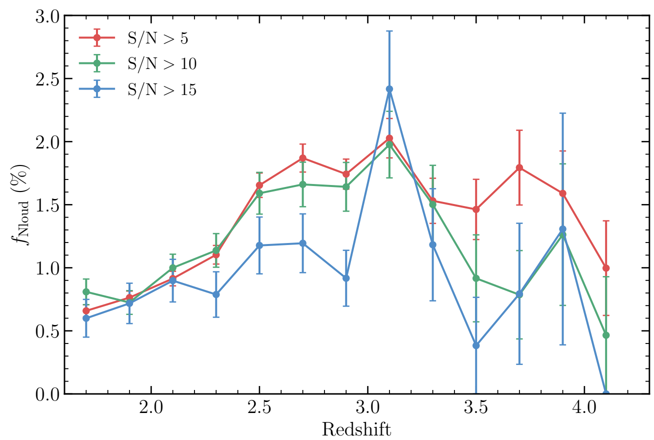

Figure 10. Redshift evolution of the N-loud fraction under different continuum S/N selections. The red, green, and blue points show the N-loud fractions measured with continuum S/N thresholds of S/N > 5, S/N > 10, and S/N > 15, respectively.

B. CONSTRUCTION OF THE SDSS CONTROL SAMPLE MATCHED TO DESI N-LOUD QUASARS

To construct a direct comparison sample for the DESI N-loud quasars, we selected SDSS control quasars matched to the DESI N-loud sample in redshift and UV continuum luminosity. We retained SDSS DR14 quasars with reliable continuum luminosity measurements by requiring `QUALITY_L1350 = 0`, and converted L_{1350} to L_{1450} assuming $f_\lambda \propto \lambda^{-1.5}$. To avoid duplicated sources, SDSS quasars within 2 arcsec of any DESI N-loud quasar were removed through sky-coordinate matching. For each DESI N-loud quasar, we then selected five nearest SDSS quasars in the redshift–$\log L_{1450}$ plane, without replacement. Figure 11 shows that the resulting SDSS control sample closely matches the DESI N-loud sample in both redshift and UV continuum luminosity, providing a suitable control sample for direct comparison with the DESI N-loud quasars in subsequent analyses.

C. N-LOUD QUASARS COMPARED WITH A DESI-PARENT-LIKE SDSS CONTROL SAMPLE

To examine the statistical properties of DESI N-loud quasars at the parent-population level, we constructed an SDSS control sample with the same redshift and 1450 Å continuum-luminosity distributions as the DESI parent quasar

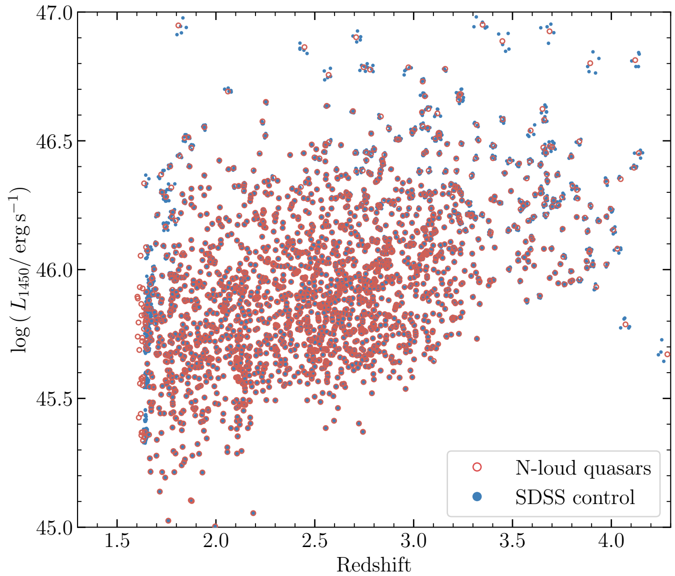

Figure 11. Redshift versus rest-frame 1450 Å luminosity distribution for the DESI N-loud quasars and the matched SDSS control sample. Red open circles denote the DESI N-loud quasars, and blue filled circles denote the SDSS control quasars selected from the SDSS DR14 quasar catalog.

sample, and compared the N-loud quasars with this control sample. We selected sources from the SDSS DR14 quasar spectral catalog with reliable bolometric luminosities and reddening corrections, requiring `QUALITY_LBOL = 0` and `QUALITY_REDD = 0`, and converted the SDSS catalog $\log L_{1350}$ measurements to $\log L_{1450}$ by assuming $f_\lambda \propto \lambda^{-1.5}$. We then constructed two-dimensional bins over $1.6 < z < 4.3$ and $44.5 < \log L_{1450} < 47.5$, with bin sizes of $\Delta z = 0.2$ and $\Delta \log L_{1450} = 0.2$. In each bin, SDSS quasars were randomly sampled without replacement according to the fractional occupancy of the DESI parent sample; the target total size was set to 50,000, with the number of sampled objects in each bin determined jointly by this fraction and the number of available SDSS sources in that bin. The resulting SDSS control sample closely matches the DESI parent sample in the overall redshift and $\log L_{1450}$ distributions, as shown in Figure 12.

Based on this DESI-parent-like SDSS control sample, we compared the emission line properties and black hole accretion properties of N-loud quasars with those of ordinary quasars. Figure 13 shows that, relative to the SDSS control sample, N-loud quasars tend to have narrower C IV and Mg II emission line widths, and their equivalent-width distributions are also systematically shifted. Figure 14 further shows that N-loud quasars are preferentially associated with lower black hole masses and higher Eddington ratios. Overall, the comparison shows that, relative to DESI-parent-like SDSS control sample, N-loud quasars show narrower broad emission lines, lower black hole masses, and higher Eddington ratios.

REFERENCES

Baldwin, J. A., Hamann, F., Korista, K. T., et al. 2003, ApJ, 583, 649, doi: 10.1086/345449

Batra, N. D., & Baldwin, J. A. 2014, MNRAS, 439, 771, doi: 10.1093/mnras/stu007

Becker, R. H., White, R. L., & Helfand, D. J. 1995, ApJ, 450, 559, doi: 10.1086/176166

Bentz, M. C., Hall, P. B., & Osmer, P. S. 2004, AJ, 128, 561, doi: 10.1086/422346

Bentz, M. C., & Osmer, P. S. 2004, AJ, 127, 576, doi: 10.1086/381299

Brodzeller, A., Dawson, K., Bailey, S., et al. 2023, AJ, 166, 66, doi: 10.3847/1538-3881/ace35d

Bunker, A. J., Saxena, A., Cameron, A. J., et al. 2023, A&A, 677, A88, doi: 10.1051/0004-6361/202346159

Coatman, L., Hewett, P. C., Banerji, M., & Richards, G. T. 2016, MNRAS, 461, 647, doi: 10.1093/mnras/stw1360

Coatman, L., Hewett, P. C., Banerji, M., et al. 2017, MNRAS, 465, 2120, doi: 10.1093/mnras/stw2797

DESI Collaboration, Aghamousa, A., Aguilar, J., et al. 2016a, arXiv e-prints, arXiv:1611.00037, doi: 10.48550/arXiv.1611.00037

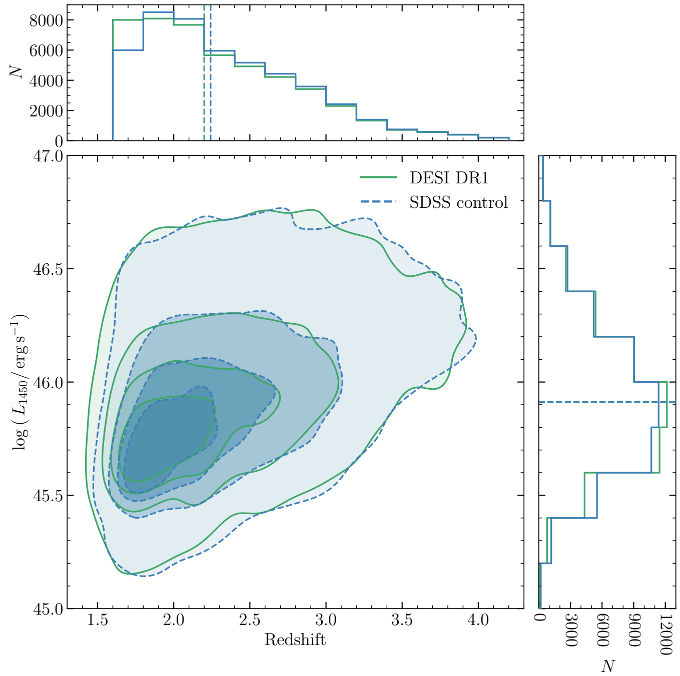

Figure 12. Redshift versus rest-frame 1450 Å luminosity distribution for the DESI DR1 parent quasar sample and the SDSS control sample. The 20%, 40%, 68%, and 95% percentile density contours are shown, with shaded regions indicating the corresponding density levels. Green solid contours represent the DESI DR1 parent quasar sample, while blue dashed contours represent the SDSS DR14 control sample. The top and right panels show the corresponding one-dimensional distributions of redshift and $\log L_{1450}$, respectively, with dashed lines indicating the median values.

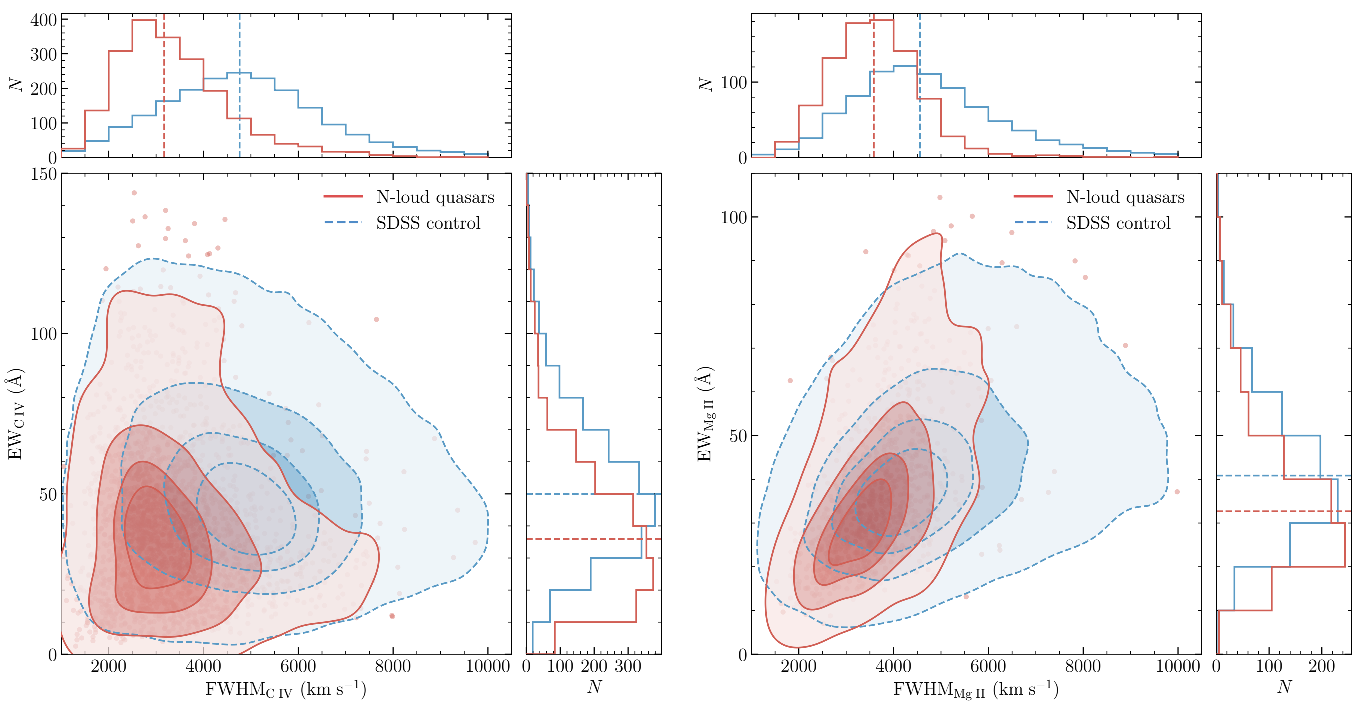

Figure 13. Rest-frame EW versus FWHM distributions of C IV (left panel) and Mg II (right panel) for the N-loud quasars (red solid contours) and SDSS DR14 control sample (blue dashed contours). Red points show individual objects. The 20%, 40%, 68%, and 95% contours and the corresponding density maps are shown. For each main panel, the top and right panels show the corresponding one-dimensional distributions of FWHM and EW, respectively, with dashed lines indicating the median values.

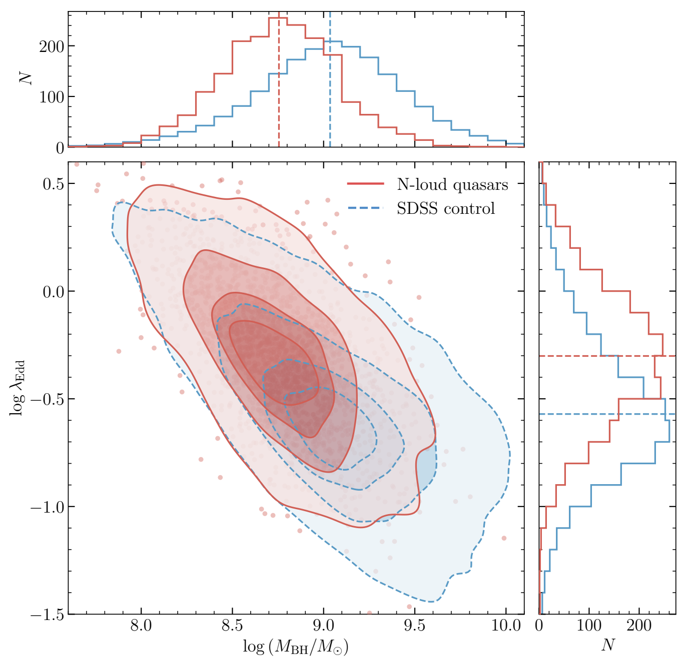

Figure 14. Black hole mass versus Eddington ratio distribution for the N-loud quasars and the SDSS control sample. The 20%, 40%, 68%, and 95% percentile density contours are shown, with shaded regions indicating the corresponding density levels. Red solid contours and points represent the N-loud quasars, while blue dashed contours represent the SDSS DR14 control sample. The top and right panels show the corresponding one-dimensional distributions of log $M_{\rm BH}$ and log $\lambda_{\rm Edd}$, respectively, with dashed lines indicating the median values.

DESI Collaboration, Aghamousa, A., Aguilar, J., et al. 2016b, arXiv e-prints, arXiv:1611.00036, doi: 10.48550/arXiv.1611.00036

DESI Collaboration, Abareshi, B., Aguilar, J., et al. 2022, AJ, 164, 207, doi: 10.3847/1538-3881/ac882b

DESI Collaboration, Karim, M. A., Adame, A. G., et al. 2025, arXiv e-prints, arXiv:2503.14745, doi: 10.48550/arXiv.2503.14745

Du, P., Brotherton, M. S., Wang, K., et al. 2018, ApJ, 869, 142, doi: 10.3847/1538-4357/aaed2c

Fitzpatrick, E. L. 1999, PASP, 111, 63, doi: 10.1086/316293

Isobe, Y., Maiolino, R., D'Eugenio, F., et al. 2025, MNRAS, 541, L71, doi: 10.1093/mnrasl/slaf056

Ji, X., Belokurov, V., Maiolino, R., et al. 2026, MNRAS, 545, staf2110, doi: 10.1093/mnras/staf2110

Ji, X., Übler, H., Maiolino, R., et al. 2024, MNRAS, 535, 881, doi: 10.1093/mnras/stae2375

Jiang, L., Fan, X., Ivezić, Ž., et al. 2007, ApJ, 656, 680, doi: 10.1086/510831

Jiang, L., Fan, X., & Vestergaard, M. 2008, ApJ, 679, 962, doi: 10.1086/587868

Lacy, M., Baum, S. A., Chandler, C. J., et al. 2020, PASP, 132, 035001, doi: 10.1088/1538-3873/ab63eb

Levi, M., Bebek, C., Beers, T., et al. 2013, arXiv e-prints, arXiv:1308.0847, doi: 10.48550/arXiv.1308.0847

Matsuoka, K., Nagao, T., Maiolino, R., et al. 2017, A&A, 608, A90, doi: 10.1051/0004-6361/201629878

Miller, T. N., Doel, P., Gutierrez, G., et al. 2024, AJ, 168, 95, doi: 10.3847/1538-3881/ad45fe

Osmer, P. S. 1980, ApJ, 237, 666, doi: 10.1086/157913

Planck Collaboration, Aghanim, N., Akrami, Y., et al. 2020, A&A, 641, A6, doi: 10.1051/0004-6361/201833910

Rakshit, S., Stalin, C. S., & Kotilainen, J. 2020, ApJS, 249, 17, doi: 10.3847/1538-4365/ab99c5

Schlafly, E. F., Kirkby, D., Schlegel, D. J., et al. 2023, AJ, 166, 259, doi: 10.3847/1538-3881/ad0832

Silber, J. H., Fagrelius, P., Fanning, K., et al. 2023, AJ, 165, 9, doi: 10.3847/1538-3881/ac9ab1

Vanden Berk, D. E., Richards, G. T., Bauer, A., et al. 2001, AJ, 122, 549, doi: 10.1086/321167

Vestergaard, M., & Osmer, P. S. 2009, ApJ, 699, 800, doi: 10.1088/0004-637X/699/1/800

Vestergaard, M., & Peterson, B. M. 2006, ApJ, 641, 689, doi: 10.1086/500572

Vestergaard, M., & Wilkes, B. J. 2001, ApJS, 134, 1, doi: 10.1086/320357